

Neural Network Construction of the Equation of State from Relativistic *ab initio* Calculations

KANGMIN CHEN,¹ XIAOYING QU,² HUI TONG,³ SIBO WANG,^{4,5} AND YANGYANG YU¹

¹*School of Physics and Mechatronic Engineering, Guizhou Minzu University, Guiyang 550025, China*

²*School of Physics and Mechatronic Engineering, Guizhou Minzu University, Guiyang 550025, China, xiaoyingqu@126.com*

³*Helmholtz-Institut für Strahlen- und Kernphysik and Bethe Center for Theoretical Physics, Universität Bonn, Bonn D-53115, Germany, tong@hiskp.uni-bonn.de*

⁴*Department of Physics and Chongqing Key Laboratory for Strongly Coupled Physics, Chongqing University, Chongqing 401331, China, sbwang@cqu.edu.cn*

⁵*Department of Physics, Graduate School of Science, The University of Tokyo, Tokyo 113-0033, Japan*

ABSTRACT

Constraining the nuclear matter equation of state (EOS) beyond saturation density is a central goal of nuclear physics and astrophysics. While the relativistic Brueckner-Hartree-Fock (RBHF) theory, an *ab initio*, non-perturbative nuclear many-body theory starting from realistic interactions, accurately describes nuclear matter properties near the saturation density $\rho_0 \approx 0.16 \text{ fm}^{-3}$, its applicability is currently limited to densities up to $3\rho_0$, necessitating a reliable extrapolation to higher densities. In this work, we employ supervised machine learning to train thousands of fully connected neural networks on low-density RBHF data. By enforcing thermodynamic consistency and smoothness, we finally select a subset of 264 optimal models. These models employ the Swish activation function, which we identify as the most reliable choice for stable extrapolation after extensive testing and comparison. Using these models to extend the EOS over the full density range, we obtain the nuclear matter symmetry energy and then compute the neutron star mass-radius relation and tidal deformability, which are in a great harmony with current astronomical observations. The corresponding extrapolation uncertainty originates from the combined contributions of both the 264 optimal models and the linear regression on nuclear matter EOS, yielding a symmetry energy of $E_{\text{sym}}(5\rho_0) = 136.0 \pm 52.8 \text{ MeV}$, a pressure of $P(5\rho_0) = 346.3 \pm 97.4 \text{ MeV/fm}^3$, a maximum neutron star mass of $M_{\text{max}} = 2.18 \pm 0.18 M_{\odot}$, and a tidal deformability of $\Lambda_{1.4M_{\odot}} = 532 \pm 34$. This work establishes a general and data-driven framework to explore dense matter EOS by integrating *ab initio* calculations with modern machine learning techniques.

1. INTRODUCTION

Understanding the equation of state (EOS) of the dense, neutron-rich matter from the fundamental interactions among its constituents remains one of the major challenges in nuclear physics and astrophysics (Danielewicz et al. 2002; Weber et al. 2007; Baldo & Burgio 2016; Lattimer & Prakash 2016; Li et al. 2018; Oertel et al. 2017; Dietrich et al. 2020; Li et al. 2020; Elhatisari et al. 2024), as it governs a wealth of phenomena over an exceptionally broad range of scales—from terrestrial heavy-ion collisions to binary neutron star mergers and core-collapse supernovae. Therefore, it has motivated major scientific initiatives and driven the development of key research infrastructures worldwide, including large ground-based telescopes, advanced space-based X-ray observatories, the Neutron Star Interior Composition Explorer (NICER), the LIGO/Virgo/KAGRA network of gravitational-wave detectors, and next-generation radioactive isotope beam facilities (Aasi et al. 2015; Acernece et al. 2015; Gendreau & Arzoumanian 2017; Akutsu et al. 2019).

Theoretically, extensive efforts have been devoted to deriving the neutron star EOS using a variety of nuclear many-body approaches, which can broadly grouped into two categories. The first category relies primarily on nuclear density functional theories (DFTs) employing effective nucleon-nucleon interactions (Yang & Piekarewicz 2020; Sedrakian et al. 2023). Because the isovector sector in most DFTs is only weakly constrained during parameters optimization, their predictions for key nuclear matter quantities, such as the symmetry energy at supra-saturation densities, remain highly uncertain (Baldo & Burgio 2016; Sorensen et al. 2024).

In contrast, the second category consists of *ab initio* methods based on realistic forces fitted directly to few-body bound and scattering data (Burgio et al. 2021; Machleidt & Sammarruca 2024; Tong et al. 2025a,b,c). Given the extreme densities reached in neutron star interiors, a Lorentz-invariant many-body treatment is particularly advantageous, as it naturally accounts for the increasingly important relativistic kinematics and dynamics. The relativistic Brueck-

ner–Hartree–Fock (RBHF) theory provides such a covariant framework (Shen et al. 2019). Built upon the relativistic Bonn potentials (Machleidt 1989), RBHF theory has been successfully applied to finite nuclei, infinite nuclear matter, and neutron star calculations (Horowitz & Serot 1984; Brockmann & Machleidt 1990; de Jong & Lenske 1998; van Dalen et al. 2005; Krastev & Sammarruca 2006; Katayama & Saito 2013; Shen et al. 2017; Tong et al. 2018, 2020), offering a unified and microscopic description of strongly interacting matter across a wide density range.

Recently, a fully self-consistent RBHF framework formulated in the full Dirac space has been developed (Wang et al. 2021), in which both the Lorentz structure and momentum dependence of the nucleon self-energy are determined without approximations. This advance resolves the long-standing inconsistencies in earlier implementations and provides a unique and accurate description of isospin effects in nuclear matter (Wang et al. 2022a, 2023, 2024; Qin et al. 2024). Despite these achievements, this self-consistent RBHF calculations of neutron star EOS (Tong et al. 2022; Wang et al. 2022a,b; Qu et al. 2025; Laskos-Patkos et al. 2025; Tong et al. 2025d) can currently be performed only up to baryon densities of about 0.5 fm^{-3} —far below the central densities of massive neutron stars. As a result, the EOS at higher densities remains theoretically inaccessible within the present self-consistent RBHF framework, and existing studies have relied primarily on parametric extrapolations rather than fully microscopic predictions.

Machine learning (ML) provides a powerful framework for function approximation and extrapolation, enabling one to capture complex nonlinear relationships in data that are difficult to model with traditional analytical methods. In nuclear physics, ML techniques have been successfully applied across the diversity of research topics, leading to advances that will facilitate scientific discoveries and offer deeper insights (Boehnlein et al. 2022; He et al. 2023; Zhou et al. 2024). In the context of nuclear matter and neutron star EOS studies, Bayesian inference techniques have been widely adopted to extract posterior distribution from terrestrial experiments, astrophysical multi-messenger observations, and microscopic nuclear theory calculations (Huth et al. 2022; Han et al. 2023; Tsang et al. 2024; Rutherford et al. 2024; Koehn et al. 2025). In parallel, neural networks (NNs) have been increasingly explored as powerful tools to infer EOS of dense nuclear matter from astrophysical observations of neutron stars (Fujimoto et al. 2018, 2020; Traversi & Char 2020; Morawski & Bejger 2020; Fujimoto et al. 2021; Ferreira & Providência 2021; Krastev 2022; Zhou et al. 2023; Fujimoto et al. 2024).

In previous applications of neural networks to neutron star studies, most efforts have focused on learning a direct mapping between the EOS and astrophysical observables such as the stellar mass–radius relation. As a consequence, these models provide limited access to

more microscopic quantities of nuclear matter, including the symmetry energy and particle fractions. Moreover, existing studies typically incorporate the two-solar-mass constraint from the outset, which effectively forces the network to cover the entire density range during training. This setup primarily tests the interpolation capability of the network, while leaving its extrapolation performance largely unexplored. To the best of our knowledge, no work to date has directly linked neural network modeling with *ab initio* nuclear matter calculations in a way that simultaneously evaluates fitting and extrapolation capabilities, and thereby yields genuine predictions for the high-density sector of the neutron star EOS.

In this work, starting from low-density datasets generated from RBHF theory in the full Dirac space, we train a neural network that predicts the binding energy per nucleon with nucleon density and isospin asymmetry as inputs. This approach enables a reliable extension of the nuclear matter EOS to high densities relevant for neutron star interiors.

This paper is organized as follows. The theoretical framework of the RBHF theory in the full Dirac space, and the preparation of the training and validation data, together with the structure and the uncertainty estimate of the neural networks, are briefly introduced in Section 2. In Section 3, the EOS, mass–radius relation, and tidal deformability of neutron star are presented. A short conclusion and outlook for future investigations are given in Section 4.

2. METHODS

2.1. Relativistic Brueckner–Hartree–Fock Theory in the Full Dirac Space

The RBHF theory provides an *ab initio* and parameter-free description of nuclear matter, where the many-body correlations are treated through the effective G -matrix. The starting point is the single-particle Dirac equation,

$$[\boldsymbol{\alpha} \cdot \mathbf{p} + \beta(M + \mathcal{U})]u(\mathbf{p}, s) = E_{\mathbf{p}}u(\mathbf{p}, s), \quad (1)$$

where $\boldsymbol{\alpha}$ and β are the Dirac matrices, M is the nucleon mass, \mathbf{p} and $E_{\mathbf{p}}$ are the momentum and single-particle energy, and s denotes the spin. The single-particle potential \mathcal{U} fully incorporates the in-medium effects.

The construction of \mathcal{U} relies on the G -matrix, which is obtained by solving the in-medium Thompson equation (Brockmann & Machleidt 1990),

$$\begin{aligned} G(\mathbf{q}', \mathbf{q}|\mathbf{P}, W) &= V(\mathbf{q}', \mathbf{q}|\mathbf{P}) + \int \frac{d^3 k}{(2\pi)^3} V(\mathbf{q}', \mathbf{k}|\mathbf{P}) \\ &\quad \times \frac{Q(\mathbf{k}, \mathbf{P})}{W - E_{\mathbf{P}+\mathbf{k}} - E_{\mathbf{P}-\mathbf{k}} + i\epsilon} \\ &\quad \times G(\mathbf{k}, \mathbf{q}|\mathbf{P}, W). \end{aligned} \quad (2)$$

Here \mathbf{P} is half of the center-of-mass momentum, and \mathbf{q} , \mathbf{k} , and \mathbf{q}' denote the initial, intermediate, and final relative momenta respectively. The Pauli operator

$Q(\mathbf{k}, \mathbf{P})$ prevents scattering into occupied intermediate states. The starting energy W is taken as the sum of the single-particle energies in the initial state. This equation resums ladder diagrams to all orders and incorporates the underlying one-boson-exchange interaction V .

As a relativistic many-body method, RBHF theory necessitates a self-consistency solution rooted in the full Dirac space. Traditional implementations restrict the scattering equation to the subspace of positive-energy states, causing ambiguities in the scalar-vector decomposition of \mathcal{U} and leading to inconsistent predictions for asymmetric nuclear matter and the symmetry energy at moderate densities.

The fully self-consistent RBHF framework in the full Dirac space developed recently overcomes these issues by treating both positive- and negative-energy states (NESs) on an equal footing (Wang et al. 2021, 2022a). This enables the construction of all matrix elements of the single-particle potential operator \mathcal{U} by summing the effective two-body G matrix over all nucleons within the Fermi sea in the full Dirac space. This full Dirac space construction allows for the exact extraction of the Lorentz structure of \mathcal{U} , which is crucial for solving the Dirac equation in the next iteration. Consequently, inclusion of the NESs has not only clarified the long-standing controversy about the isospin dependence of the effective mass in neutron-rich matter (Wang et al. 2022a), but also yielded a fully consistent determination of the single-particle spectrum (Wang et al. 2023) and the in-medium interaction (Wang et al. 2025).

With the converged Dirac spinor and G -matrix, the binding energy per nucleon of nuclear matter is calculated by

$$\begin{aligned} E/A = & \frac{1}{\rho} \int_{\mathbf{p}} \langle \bar{u}(\mathbf{p}) | \gamma \cdot \mathbf{p} + M | u(\mathbf{p}) \rangle - M \\ & + \frac{1}{2\rho} \int_{\mathbf{p}} \int_{\mathbf{p}'} \langle \bar{u}(\mathbf{p}) \bar{u}(\mathbf{p}') | \bar{G}(W) | u(\mathbf{p}) u(\mathbf{p}') \rangle. \end{aligned} \quad (3)$$

Here, the density ρ is related to the Fermi momentum k_F through $\rho = 2k_F^3/3\pi^2$, $\int_{\mathbf{p}} \equiv \int_0^{k_F} d^3p/(2\pi)^3$, $W = E_{\mathbf{p}} + E_{\mathbf{p}'}$, and the spin as well as isospin indices are suppressed. More theoretical and numerical details are provided in Wang et al. (2021, 2022a); Tong et al. (2022).

In the vicinity of the nuclear saturation density, the binding energy per nucleon of asymmetric nuclear matter (ANM) can be generally expressed as a power series in the asymmetry parameter $\alpha = (\rho_n - \rho_p)/\rho$, with ρ_n, ρ_p , and $\rho = \rho_n + \rho_p$ being the neutron, proton, and nucleon density, respectively (Bombaci & Lombardo 1991):

$$E/A(\rho, \alpha) = E_{\text{SNM}}(\rho) + E_{\text{sym}}(\rho)\alpha^2 + \mathcal{O}(\alpha^4). \quad (4)$$

Here, $E_{\text{SNM}}(\rho) = E/A(\rho, 0)$ is the binding energy per nucleon of symmetric nuclear matter (SNM), and $E_{\text{sym}}(\rho)$ is the density-dependent symmetry energy.

Presently, the EOS of cold nuclear matter under extreme conditions of density and isospin asymmetry still remains rather uncertain and theoretically controversial, particularly at supra-saturation densities and with extreme neutron abundance, mainly due to the poorly known high-density behavior of the nuclear symmetry energy $E_{\text{sym}}(\rho)$ (Li et al. 2014, 2021). The RBHF theory formulated in the full Dirac space thus provides a unique and ambiguity-free microscopic description of nuclear matter up to densities $\rho \approx 0.5 \text{ fm}^{-3}$. This makes it an ideal generator of high-fidelity, first-principle data, enabling our ML model to extrapolate the EOS into the high-density region relevant for neutron star interiors.

2.2. Training and Validation Data

The neutral networks developed in this work are trained on high-fidelity datasets generated from the fully self-consistent RBHF calculations in the full Dirac space. These *ab initio* calculations are computationally demanding and can only be stably converged up to densities $\rho \approx 0.52 - 0.57 \text{ fm}^{-3}$, depending on the isospin asymmetry (Wang et al. 2022a). Owing to its larger Fermi momentum, pure neutron matter reaches its maximum attainable density at a lower value than SNM. As the computational cost increases sharply with the increase in density, the available dataset is sparse in density and uneven in α , while remaining extremely reliable in the converged region. This motivates a training strategy explicitly designed to preserve the predictive power of the RBHF inputs while enabling controlled extrapolation.

The data are sampled on a fixed density grid,

$$\rho_i = 0.08 + 0.01i \text{ fm}^{-3}, \quad i = 0, 1, \dots, i_{\text{max}}, \quad (5)$$

extending slightly above 0.5 fm^{-3} , and on eleven asymmetry parameters

$$\alpha_j = 0.1j, \quad j = 0, 1, \dots, 10. \quad (6)$$

For every sampled pair (ρ_i, α_j) , the corresponding binding energy per nucleon $E/A(\rho_i, \alpha_j)$ is obtained. In total, around 530 converged points are available.

Since the ultimate goal is to extrapolate the EOS into the high-density regime relevant for neutron star interiors, the dataset must allow us to rigorously assess the model's robustness specifically under high densities and large isospin asymmetry. To this end, the partition of training and validation sets is constructed as follows:

$$\begin{aligned} \mathcal{D}_{\text{train}} = & \{E/A(\rho, \alpha) | \alpha \leq 0.7, \rho \leq 0.5 \text{ fm}^{-3}\} \\ & \cup \{E/A(\rho, \alpha) | \alpha \geq 0.8, \rho \leq 0.45 \text{ fm}^{-3}\}, \\ \mathcal{D}_{\text{validation}} = & \text{remaining data with larger } \rho \text{ at each } \alpha. \end{aligned} \quad (7)$$

This partitioning yields 458 and 72 data points for the training and validation sets, respectively. Both density ρ and isospin asymmetry α are rescaled to the interval $[-1, 1]$ for numerical stability, and the binding energy per nucleon is normalized by a constant scale. No

smoothing, fitting, or interpolation is applied and the neural network learns directly from the raw RBHF calculations. This preserves the *ab initio* nature of the input and ensures that all features learned by the model originate from the underlying microscopic theory.

2.3. Neural Network Architecture

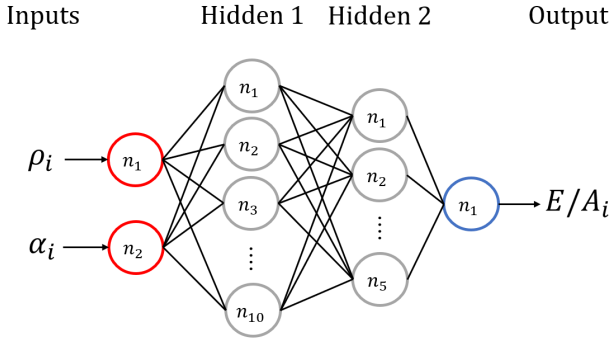


Figure 1. Schematic illustration of the feedforward neural network.

To emulate the density and isospin dependence of the RBHF EOS, we construct a fully connected neural network that maps the two physical input variables, the nucleon density ρ and the isospin asymmetry α , to a single output, the binding energy per nucleon $E/A(\rho, \alpha)$. The architecture of our neural network is illustrated in Figure 1, consisting of an input layer with two neurons, two hidden layers with 10 and 5 neurons respectively, and a single-neuron output layer. All networks in the ensemble share this structure, differing only in the realization of randomly initialized weights and biases.

Unlike many applications of ML where the choice of activation function impacts only performance, in our case the activation function plays a central physical role: it governs whether the learned EOS can be meaningfully extrapolated to densities beyond the RBHF convergence limit. The activation function must therefore satisfy two criteria: (1) The network must accurately learn the smooth dependence of $E/A(\rho, \alpha)$ encoded in the RBHF data across the sampled range of densities and asymmetries. (2) When extended to higher densities relevant for neutron star interiors, the pressure $P(\rho)$ inferred from the neural work must obey: (i) Thermodynamic stability $dP/d\rho > 0$; (ii) smoothness since our model contains neither phase transitions nor additional degrees of freedom.

These stringent physical conditions significantly constrain the choice of viable activation functions. We therefore conducted a systematic evaluation of com-

monly used activation functions including ReLu, Sigmoid, and Tanh. In addition, we also test the Swish activation function (Ramachandran et al. 2018),

$$\text{Swish}(x) = x \cdot \frac{1}{1 + e^{-\beta x}}, \quad (8)$$

which is not commonly used in EOS-related neural network studies. We set $\beta = 1$ in this work (Ramachandran et al. 2018). Each activation function was evaluated based on its accuracy on the RBHF training and validation data at low and moderate densities and the physical plausibility of the extrapolated EOS at high densities. The computations are performed in Python, employing Keras (Chollet 2015) with TensorFlow (Abadi et al. 2016) as the backend. For optimization, the Adam algorithm (Kingma & Ba 2017) is adopted with a batch size of 32, and the mean squared error is adopted as the loss function.

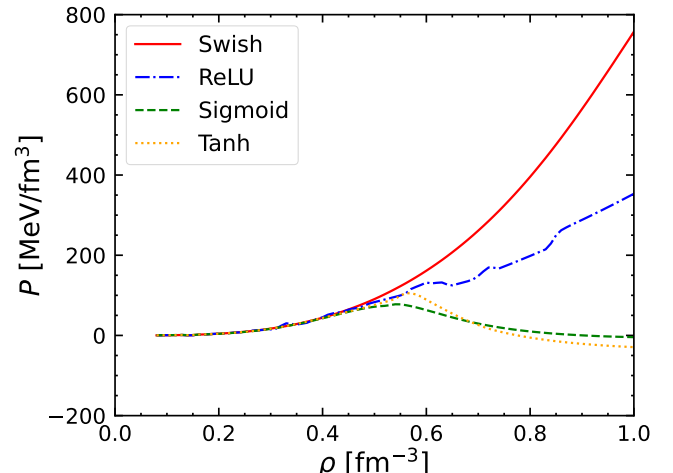


Figure 2. Pressure of neutron star matter as a function of nucleon number density obtained using four activation functions: Swish (red solid line), ReLU (blue dash-dotted line), Sigmoid (green dashed line) and Tanh (orange dotted line). The white area indicates the part of the dataset used for training, whereas the gray-shaded area represents the extrapolation region where the model predictions are evaluated.

Figure 2 depicts the pressure of neutron star matter as a function of nucleon density calculated with $E/A(\rho, \alpha)$ obtained with four activation functions. Our tests reveal that the Swish activation function offers distinctly superior extrapolation behavior. ReLU networks tend to produce non-smooth pressures and even thermodynamic instabilities, and Sigmoid/Tanh saturate too rapidly to represent the high-density rise of the EOS. In comparison, Swish network captures the continuous growth of the nuclear matter EOS at supra-saturation densities, which potentially corresponds to the repulsive behavior of nucleon-nucleon interactions in the high-density region. As shown in Figure 2, only Swish yields an

EOS that remains smooth and thermodynamically stable throughout the extrapolation region. Consequently, all neural networks selected for the final ensemble employ Swish in all hidden layers.

The superior performance of the Swish activation function is attributed to its ability to mitigate critical flaws in both ReLU and saturation functions like Sigmoid/Tanh. Specifically, it circumvents the instability and neuron "death" associated with ReLU during extrapolation and, unlike Sigmoid/Tanh, does not suffer from complete gradient vanishing in unseen data regions (Apicella et al. 2021; Goodfellow et al. 2016). Consequently, Swish exhibits substantially more stable and robust predictive behavior. Furthermore, its global smoothness and full differentiability make it a more effective alternative than ReLU, Sigmoid, or Tanh for tasks that require robust generalization and accurate predictions beyond the training data distribution.

2.4. Uncertainty Estimation

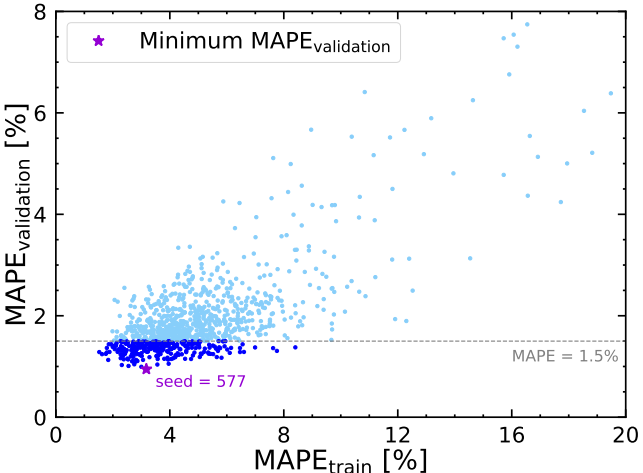


Figure 3. Distribution and selection of 1000 neural networks based on MAPE. The dashed line indicates the 1.5% validation MAPE threshold. Minimum validation MAPE (0.95%) achieved by the neural network with random seed 577 is marked with a purple star.

The stochastic initialization of weights and biases during neural network training inevitably introduces a degree of randomness into the model, leading to slightly different mappings across different training runs. To quantify the resulting model uncertainty and ensure reproducibility, we construct an ensemble of 1000 independently trained neural networks, each initialized with a distinct but fixed random seed. For every model in the ensemble, we evaluate the agreement with the RBHF data using the mean absolute percentage error (MAPE),

$$\text{MAPE} = \frac{1}{N} \sum_{i=1}^N \left| \frac{(E/A)_{\text{NN},i} - (E/A)_{\text{RBHF},i}}{(E/A)_{\text{RBHF},i}} \right|, \quad (9)$$

where the sum runs over the N data points. This metric provides a dimensionless and robust measure of the model's extrapolation accuracy, independent of the absolute scale of the binding energy.

The distribution of MAPE values for the training and validation sets across the ensemble is shown in Figure 3. A clear positive correlation is observed. Neural networks those fit the training data more accurately also exhibit smaller validation errors, indicating that overfitting is negligible and the learned functional dependence is physically robust. To isolate models with reliable extrapolation behavior, we impose a threshold $\text{MAPE}_{\text{validation}} \leq 1.5\%$. In total 264 neural networks satisfy this criterion, and only these are retained for all subsequent predictions of the symmetry energy, pressure, and neutron star observables. Notably, the neural network corresponding to random seed 577 yields the minimum validation MAPE (0.95%) and is indicated by a purple star in Figure 3. The spread among this selected ensemble provides a direct statistical estimate of the theoretical uncertainty associated with the ML extrapolation.

3. RESULTS AND DISCUSSIONS

The exceptional extrapolative capability of our neural network model, demonstrated through its predictions of the binding energy per nucleon across a wide density range, paves the way for a unified calculation of key nuclear and astrophysical properties. This enables us to derive the nuclear matter symmetry energy from low to high densities, the neutron star matter pressure, and critical neutron star observables—encompassing the mass-radius relation and tidal deformability.

It should be emphasized that the neural networks are trained to predict the binding energy per nucleon $E/A(\rho, \alpha)$ for arbitrary density and isospin asymmetry. To obtain the symmetry energy at a fixed density, we perform a linear regression fitting the machine-learning predictions to the quadratic expansion in Equation (4). This regression approach makes use of the full information provided by the neural network EOS with eleven asymmetry values $\alpha = 0, 0.1, \dots, 1.0$, thus avoids relying solely on the two extreme points with the commonly used approximation $E_{\text{sym}}(\rho) \approx E/A(\rho, \alpha = 1) - E/A(\rho, \alpha = 0)$, which becomes worse for higher densities (Wang et al. 2020). In addition, the residual contribution from high-order terms in Equation (4) is effectively incorporated into the statistical uncertainty of the fitted coefficient. As a result, the extracted $E_{\text{sym}}(\rho)$ is more robust, less biased, and more faithful to the underlying functional dependence learned by the neural networks.

The resulting symmetry energy curves for the selected ensemble (blue dots in Figure 3) are shown as blue lines in Figure 4. Up to $\rho \approx 0.5 \text{ fm}^{-3}$ where RBHF calculations provide direct microscopic input, the predictions from different neural networks are nearly indistin-

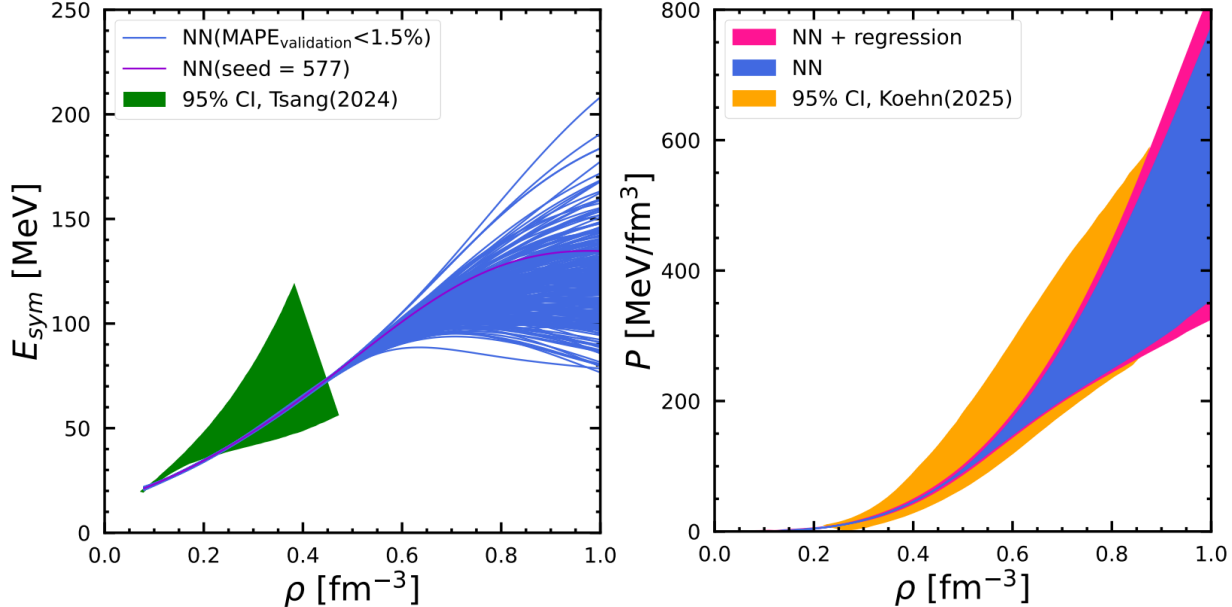


Figure 4. Left Panel: Nuclear matter symmetry energy E_{sym} as a function of density ρ . The blue solid lines denote the neural networks satisfying $\text{MAPE}_{\text{validation}} \leq 1.5\%$, while the purple solid line denotes the one with the minimum $\text{MAPE}_{\text{validation}}$. The green shaded regions represent 95% confidence interval (CI) of the posterior distributions from Tsang et al. (2024). Right Panel: Neutron star matter pressure P as a function of density ρ . The blue shaded region corresponds to the uncertainty obtained from the neural networks with $\text{MAPE}_{\text{validation}} \leq 1.5\%$, while the red shaded regions correspond to the 95% CI of E_{sym} , derived from the simple linear regression in Equation (4). The orange shaded regions correspond to the 95% CI of the posterior distribution from Koehn et al. (2025).

guishable, indicating that the regression reliably captures the RBHF trend. Our calculations are also comparable to the results of Bayesian inference that incorporate astronomical observations and nuclear experimental constraints (Tsang et al. 2024). Beyond 0.5 fm^{-3} , however, the spread among the models grows rapidly, reflecting the well-known difficulty of constraining the symmetry energy at supra-saturation densities. Up to 0.8 fm^{-3} , although a small number of neural networks predict a saturation or even a mild decline of at very high densities, the majority exhibit a steadily increasing trend. Such behavior is consistent with expectations from microscopic Brueckner–Hartree–Fock calculations based on realistic nuclear interactions as well as from relativistic mean-field models employing phenomenological forces (Li et al. 2008). The growing dispersion in the extrapolated region therefore quantifies the current theoretical uncertainty. Specifically, the symmetry energy at empirical and twice saturation density are $E_{\text{sym}}(\rho_0) = 29.4 \pm 0.3 \text{ MeV}$, $E_{\text{sym}}(2\rho_0) = 51.6 \pm 3.4 \text{ MeV}$, respectively. Both are in agreement with experimental constraints $E_{\text{sym}}(\rho_0) = 31.7 \pm 3.2 \text{ MeV}$ (Oertel et al. 2017) and $E_{\text{sym}}(2\rho_0) = 55.6 \pm 4.8 \text{ MeV}$ from ASY-EOS (Russotto et al. 2016). Extending to five times saturation density, our neural networks studies predict $E_{\text{sym}}(5\rho_0) = 136.0 \pm 52.8 \text{ MeV}$, which is left to be compared with other theoretical or experimental studies.

Based on the density dependent symmetry energy obtained above, we next construct the pressure of cold β -equilibrated neutron star matter. For each neural-network EOS, particle fractions are determined by solving simultaneously the conditions of chemical equilibrium and charge neutrality. With the composition fixed, the total energy density and pressure are computed in the standard way.

The resulting pressure bands are shown in the right panel of Figure 4. Two types of uncertainties are displayed: the blue band reflects the spread among the selected neural networks alone, while the red band includes, in addition, the statistical uncertainty associated with the linear regression used to extract the symmetry energy at each density. It is evident that the neural network variability dominates the total uncertainty, while the contribution from the regression analysis is comparatively small. Qualitatively, all selected models predict a monotonically increasing pressure with density and show no sign of saturation even at the highest densities considered. This behavior is consistent with the thermodynamic-stability criterion imposed when selecting the activation function: the extrapolated EOS must be stable and remain smooth in the absence of phase transitions or additional degrees of freedom. Below 0.8 fm^{-3} , our results fall well within the Bayesian posterior distributions (specifically, Set A) of Koehn et al. (2025), which were derived by incorporating con-

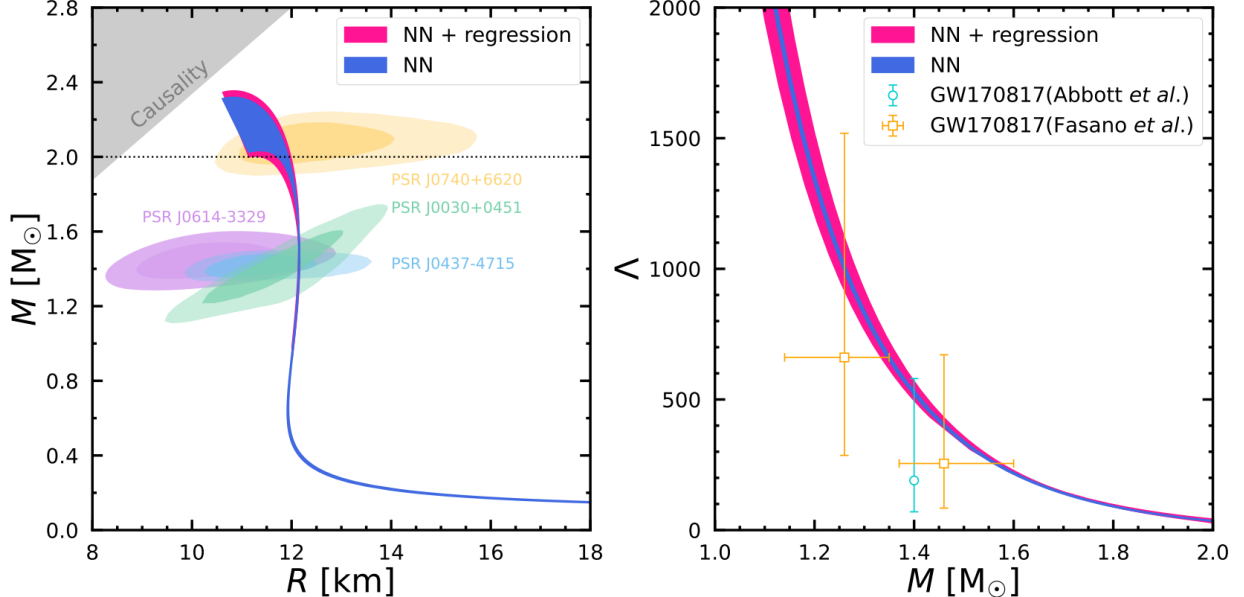


Figure 5. Left Panel: Neutron star mass-radius relation. The blue and red bands represent the uncertainties from the neural networks alone and from the combined NN and linear regression, respectively. The horizontal dotted line marks $2M_{\odot}$. The inner and outer shaded contours indicate the mass-radius constraints from NICER’s analysis of PSR J0030+0451 (Vinciguerra et al. 2024), PSR J0740+6620 (Salmi et al. 2024), PSR J0437-4715 (Choudhury et al. 2024), and PSR J0614-3329 (Mauviard et al. 2025). Right Panel: Neutron star tidal deformability Λ as a function of mass. Our results (blue and red regions) are compared with the tidal deformabilities for the two neutron stars in the merger event GW170817 as reported in Fasano et al. (2019) (open squares), as well as the value of $\Lambda_{1.4M_{\odot}}$ extracted from GW170817 (Abbott et al. 2018) (open circle).

straints from microscopic theoretical calculations and multi-messenger astronomy observations with minimal model dependence. Quantitatively, our pressure at five times the empirical saturation density is found to be $P(5\rho_0) = 346.3 \pm 97.4$ MeV/fm³.

With the EOS of β -equilibrated neutron star matter established in the previous section supplemented with BPS-BBP model (Baym et al. 1971; Baym et al. 1971) for the crust, we compute the stellar structure by solving the Tolman–Oppenheimer–Volkoff (TOV) equations for hydrostatic equilibrium. In parallel, the dimensionless tidal deformability Λ is obtained by integrating the standard first-order differential equation describing quadrupolar metric perturbations, coupled to the TOV background. Together, these solutions yield the mass–radius relation and tidal deformabilities corresponding to each neural network EOS, as shown in Figure 5.

For the mass–radius relation (left panel), the maximum mass supported by the ensemble is $2.18 \pm 0.18M_{\odot}$, including both the neural network and linear regression uncertainties. Although the uncertainty band is relatively broad, it is noteworthy that all neural networks predict a maximum mass above $2.0M_{\odot}$, fully consistent with the heavy pulsars observed in radio timing measurements (Salmi et al. 2024; Demorest et al. 2010; Fonseca et al. 2016; Arzoumanian et al. 2018). This agreement confirms that the neural networks remain stable

and physically reliable during extrapolation to the high-density regime where no RBHF data are available.

At canonical mass, the radius of a $1.4M_{\odot}$ neutron star is predicted to lie within a very narrow range around $R_{1.4M_{\odot}} = 12$ km, reflecting the fact that its central density ≈ 0.46 fm⁻³ (Tong et al. 2022), does not exceed the region where the selected neural networks show appreciable divergence. In contrast, the radius at $2.0M_{\odot}$ is found to be $R_{2.0M_{\odot}} = 11.8 \pm 0.3$ km, which spans a noticeably wider interval, since these stars probe the higher-density regime above $5 - 6\rho_0$ where extrapolation uncertainties naturally increase. Importantly, the mass–radius curves remain fully compatible with the NICER measurements of PSR J0030+0451 (Vinciguerra et al. 2024), PSR J0740+6620 (Salmi et al. 2024), PSR J0437-4715 (Choudhury et al. 2024), and PSR J0614-3329 (Mauviard et al. 2025), as illustrated by the observational contours in Figure 5. Therefore, the RBHF-trained machine learning EOS provides a realistic description of dense matter, as it leverages the high fidelity of RBHF at low and intermediate densities and maintains reliable extrapolation to higher densities through the use of physically motivated activation function.

The right panel of Figure 5 displays the corresponding tidal deformabilities. The tidal deformability Λ quantifies the ease with which a neutron star develops a quadrupole moment in response to an external

tidal field, and is therefore a key observable in multi-messenger astronomy (Abbott et al. 2017). At present, GW170817 remains the only binary neutron star merger from which Λ constraints have been obtained. Since gravitational-wave observations determine primarily the chirp mass, the inferred constraints appear as a joint allowed region for the two stellar masses and their tidal deformabilities. Our neural network predictions fall squarely within this allowed region, demonstrating consistency with current observational limits.

For $1.4M_{\odot}$ neutron star, we obtain $\Lambda_{1.4M_{\odot}} = 532 \pm 34$, lying toward the upper edge of the GW170817 constraint $\Lambda_{1.4M_{\odot}} = 190^{+390}_{-120}$ (Abbott et al. 2018). This placement indicates that the gravitational-wave analysis tends to favor a comparatively soft EOS at low densities, producing smaller stellar radii and hence smaller tidal deformabilities. When combined with the observational requirement that the EOS must also support neutron stars of at least $2.0M_{\odot}$, a picture emerges that EOS must undergo a relatively rapid stiffening between the densities characteristic of canonical mass stars and those associated with the most massive neutron stars. Such a transition from low-density softness to high-density hardness is one of the most intriguing and currently unresolved features in neutron star matter research.

To better represent the regime where EOS uncertainties become most significant, we also quote the deformability of a $2.0M_{\odot}$ neutron star, for which the central density reaches into the extrapolated domain: $\Lambda_{2.0M_{\odot}} = 31 \pm 10$. Future gravitational-wave detections of heavier binary systems will be essential for constraining this high-density region and clarifying whether the rapid stiffening suggested by current multi-messenger data is indeed a robust feature of dense matter.

4. CONCLUSIONS

We present a neural network construction of the equation of state (EOS) based on relativistic *ab initio* input. By training an ensemble of networks on relativistic Brueckner-Hartree-Fock (RBHF) data and imposing physical constraints, we obtain an EOS that is consistent with microscopic calculations at low and intermediate density and provides a stable, causal extension to the high-density region. The success of this extrapolation hinges on the use of the Swish activation function.

The density dependence of the symmetry energy, extracted through a regression analysis of the machine-learned EOS, exhibits excellent consistency among neural networks up to $\rho = 0.5 \text{ fm}^{-3}$. Beyond this region, the model spread increases, reflecting the intrinsic uncertainty of the high-density symmetry energy. The pressure of cold β -equilibrated matter, obtained after solving chemical-equilibrium and charge-neutrality conditions, shows that the neural network variation dominates the total uncertainty.

When applied to neutron star structure, the extended EOS supports maximum masses above $2.0M_{\odot}$ and yields mass-radius relations fully compatible with NICER observations. The predicted tidal deformabilities also fall within the broad range inferred from GW170817, with $\Lambda_{1.4M_{\odot}}$ lying near the upper envelope of the allowed interval, consistent with a relatively soft low-density EOS that must stiffen rapidly to support heavy neutron stars. Such a soft-to-stiff transition is a notable feature of current multi-messenger-constrained EOSs.

Our results demonstrate that combining relativistic *ab initio* input with physically constrained machine-learning extrapolation provides a robust and predictive framework for dense-matter studies. Moreover, this methodology can be readily extended to incorporate other *ab initio* calculations based on chiral effective field theory. This extension would facilitate reliable extrapolations across density regions and contribute to a unified microscopic understanding of the neutron star EOS.

5. ACKNOWLEDGMENTS

HT acknowledges funding by the European Research Council (ERC) under the European Union’s Horizon 2020 research and innovation programme (AdG EXOTIC, Grant agreement No. 101018170) and by the MKW NRW under the funding code NW21-024-A. This work was partly supported by the National Natural Science Foundation of China under Grant Nos. 12205030, 12575130, 12265012, Chongqing Natural Science Foundation under Grant No. CSTB2025NSCQ-GPX0742, and Project of Guizhou Provincial Department of Science and Technology under Grant No. CXTD[2025]030. Part of this work was achieved by using the supercomputer OCTOPUS at the Cybermedia Center, Osaka University under the support of Research Center for Nuclear Physics of Osaka University.

REFERENCES

Aasi, J., Abbott, B. P., Abbott, R., et al. 2015, Classical and Quantum Gravity, 32, 074001, doi: [10.1088/0264-9381/32/7/074001](https://doi.org/10.1088/0264-9381/32/7/074001)

Abadi, M., Barham, P., Chen, J., et al. 2016, TensorFlow: A system for large-scale machine learning. <https://arxiv.org/abs/1605.08695>

Abbott, B., Abbott, R., Abbott, T., et al. 2017, Physical Review Letters, 119, doi: [10.1103/physrevlett.119.161101](https://doi.org/10.1103/physrevlett.119.161101)

—. 2018, Physical Review Letters, 121, doi: [10.1103/physrevlett.121.161101](https://doi.org/10.1103/physrevlett.121.161101)

Acerneze, F., Agathos, M., Agatsuma, K., et al. 2015, Classical and Quantum Gravity, 32, 024001, doi: [10.1088/0264-9381/32/2/024001](https://doi.org/10.1088/0264-9381/32/2/024001)

Akutsu, T., Ando, M., Arai, K., et al. 2019, *Nature Astronomy*, 3, 35, doi: [10.1038/s41550-018-0658-y](https://doi.org/10.1038/s41550-018-0658-y)

Apicella, A., Donnarumma, F., Isgrò, F., & Prevete, R. 2021, *Neural Networks*, 138, 14, doi: <https://doi.org/10.1016/j.neunet.2021.01.026>

Arzoumanian, Z., Brazier, A., Burke-Spolaor, S., et al. 2018, *The Astrophysical Journal Supplement Series*, 235, 37, doi: [10.3847/1538-4365/aab5b0](https://doi.org/10.3847/1538-4365/aab5b0)

Baldo, M., & Burgio, G. 2016, *Progress in Particle and Nuclear Physics*, 91, 203, doi: <https://doi.org/10.1016/j.ppnp.2016.06.006>

Baym, G., Bethe, H. A., & Pethick, C. J. 1971, *Nuclear Physics A*, 175, 225, doi: [https://doi.org/10.1016/0375-9474\(71\)90281-8](https://doi.org/10.1016/0375-9474(71)90281-8)

Baym, G., Pethick, C., & Sutherland, P. 1971, *ApJ*, 170, 299, doi: [10.1086/151216](https://doi.org/10.1086/151216)

Boehnlein, A., Diefenthaler, M., Sato, N., et al. 2022, *Rev. Mod. Phys.*, 94, 031003, doi: [10.1103/RevModPhys.94.031003](https://doi.org/10.1103/RevModPhys.94.031003)

Bombaci, I., & Lombardo, U. 1991, *Physical review C: Nuclear physics*, 44, 1892, doi: [10.1103/PhysRevC.44.1892](https://doi.org/10.1103/PhysRevC.44.1892)

Brockmann, R., & Machleidt, R. 1990, *Phys. Rev. C*, 42, 1965, doi: [10.1103/PhysRevC.42.1965](https://doi.org/10.1103/PhysRevC.42.1965)

Burgio, G., Schulze, H.-J., Vidaña, I., & Wei, J.-B. 2021, *Progress in Particle and Nuclear Physics*, 120, 103879, doi: <https://doi.org/10.1016/j.ppnp.2021.103879>

Chollet, F. 2015, “Keras: Deep learning library for theano and tensorflow.”. <https://github.com/keras-team/keras>

Choudhury, D., Salmi, T., Vinciguerra, S., et al. 2024, *The Astrophysical Journal Letters*, 971, L20, doi: [10.3847/2041-8213/ad5a6f](https://doi.org/10.3847/2041-8213/ad5a6f)

Danielewicz, P., Lacey, R., & Lynch, W. G. 2002, *Science*, 298, 1592, doi: [10.1126/science.1078070](https://doi.org/10.1126/science.1078070)

de Jong, F., & Lenske, H. 1998, *Physical Review C*, 57, 3099, doi: [10.1103/PhysRevC.57.3099](https://doi.org/10.1103/PhysRevC.57.3099)

Demorest, P. B., Pennucci, T., Ransom, S. M., Roberts, M. S. E., & Hessels, J. W. T. 2010, *Nature*, 467, 1081–1083, doi: [10.1038/nature09466](https://doi.org/10.1038/nature09466)

Dietrich, T., Coughlin, M. W., Pang, P. T. H., et al. 2020, *Science*, 370, 1450, doi: [10.1126/science.abb4317](https://doi.org/10.1126/science.abb4317)

Elhatisari, S., et al. 2024, *Nature*, 630, 59, doi: [10.1038/s41586-024-07422-z](https://doi.org/10.1038/s41586-024-07422-z)

Fasano, M., Abdelsalhin, T., Maselli, A., & Ferrari, V. 2019, *Physical review letters*, 123 14, 141101. <https://api.semanticscholar.org/CorpusID:119079454>

Ferreira, M., & Providência, C. 2021, *Journal of Cosmology and Astroparticle Physics*, 2021, 011, doi: [10.1088/1475-7516/2021/07/011](https://doi.org/10.1088/1475-7516/2021/07/011)

Fonseca, E., Pennucci, T. T., Ellis, J. A., et al. 2016, *The Astrophysical Journal*, 832, 167, doi: [10.3847/0004-637x/832/2/167](https://doi.org/10.3847/0004-637x/832/2/167)

Fujimoto, Y., Fukushima, K., Kamata, S., & Murase, K. 2024, *Physical Review D*, 110, doi: [10.1103/PhysRevD.110.034035](https://doi.org/10.1103/PhysRevD.110.034035)

Fujimoto, Y., Fukushima, K., & Murase, K. 2018, *Phys. Rev. D*, 98, 023019, doi: [10.1103/PhysRevD.98.023019](https://doi.org/10.1103/PhysRevD.98.023019)

—. 2020, *Phys. Rev. D*, 101, 054016, doi: [10.1103/PhysRevD.101.054016](https://doi.org/10.1103/PhysRevD.101.054016)

—. 2021, *Journal of High Energy Physics*, 2021, doi: [10.1007/JHEP03\(2021\)273](https://doi.org/10.1007/JHEP03(2021)273)

Gendreau, K., & Arzoumanian, Z. 2017, *Nature Astronomy*, 1, doi: [10.1038/s41550-017-0301-3](https://doi.org/10.1038/s41550-017-0301-3)

Goodfellow, I., Bengio, Y., & Courville, A. 2016, *Deep Learning* (MIT Press). <http://www.deeplearningbook.org>

Han, M.-Z., Huang, Y.-J., Tang, S.-P., & Fan, Y.-Z. 2023, *Science Bulletin*, 68, 913, doi: <https://doi.org/10.1016/j.scib.2023.04.007>

He, W., Li, Q., Ma, Y., et al. 2023, *Science China Physics, Mechanics & Astronomy*, 66, 282001, doi: [10.1007/s11433-023-2116-0](https://doi.org/10.1007/s11433-023-2116-0)

Horowitz, C. J., & Serot, B. D. 1984, *Physics Letters B*, 137, 287, doi: [https://doi.org/10.1016/0370-2693\(84\)91717-9](https://doi.org/10.1016/0370-2693(84)91717-9)

Huth, S., Pang, P. T. H., Tews, I., et al. 2022, *Nature*, 606, 276, doi: [10.1038/s41586-022-04750-w](https://doi.org/10.1038/s41586-022-04750-w)

Katayama, T., & Saito, K. 2013, *Physical Review C*, 88, 035805, doi: [10.1103/PhysRevC.88.035805](https://doi.org/10.1103/PhysRevC.88.035805)

Kingma, D. P., & Ba, J. 2017, *Adam: A Method for Stochastic Optimization*. <https://arxiv.org/abs/1412.6980>

Koehn, H., Rose, H., Pang, P. T. H., et al. 2025, *Phys. Rev. X*, 15, 021014, doi: [10.1103/PhysRevX.15.021014](https://doi.org/10.1103/PhysRevX.15.021014)

Krastev, P. 2022, *Galaxies*, 10, doi: [10.3390/galaxies10010016](https://doi.org/10.3390/galaxies10010016)

Krastev, P. G., & Sammarruca, F. 2006, *Physical Review C*, 74, 025808, doi: [10.1103/PhysRevC.74.025808](https://doi.org/10.1103/PhysRevC.74.025808)

Laskos-Patkos, P., Lalazissis, G. A., Wang, S., et al. 2025, *Phys. Rev. C*, 111, 025801, doi: [10.1103/PhysRevC.111.025801](https://doi.org/10.1103/PhysRevC.111.025801)

Lattimer, J. M., & Prakash, M. 2016, *Physics Reports*, 621, 127, doi: <https://doi.org/10.1016/j.physrep.2015.12.005>

Li, A., Zhu, Z.-Y., Zhou, E.-P., et al. 2020, *Journal of High Energy Astrophysics*, 28, 19, doi: <https://doi.org/10.1016/j.jheap.2020.07.001>

Li, B.-A., Cai, B.-J., Chen, L.-W., & Xu, J. 2018, *Progress in Particle and Nuclear Physics*, 99, 29, doi: <https://doi.org/10.1016/j.ppnp.2018.01.001>

Li, B.-A., Cai, B.-J., Xie, W.-J., & Zhang, N.-B. 2021, Universe, 7, doi: [10.3390/universe7060182](https://doi.org/10.3390/universe7060182)

Li, B.-A., Chen, L.-W., & Ko, C. M. 2008, Physics Reports, 464, 113, doi: <https://doi.org/10.1016/j.physrep.2008.04.005>

Li, B.-A., Ramos, Á., Verde, G., & Vidaña, I. 2014, The European Physical Journal A, 50, <https://api.semanticscholar.org/CorpusID:254114709>

Machleidt, R. 1989, The Meson Theory of Nuclear Forces and Nuclear Structure (Boston, MA: Springer US), 189–376, doi: [10.1007/978-1-4613-9907-0_2](https://doi.org/10.1007/978-1-4613-9907-0_2)

Machleidt, R., & Sammarruca, F. 2024, Progress in Particle and Nuclear Physics, 137, 104117, doi: <https://doi.org/10.1016/j.ppnp.2024.104117>

Mauviard, L., Guillot, S., Salmi, T., et al. 2025, A NICER view of the 1.4 solar-mass edge-on pulsar PSR J0614–3329. <https://arxiv.org/abs/2506.14883>

Morawski, F., & Bejger, M. 2020, Astronomy and Astrophysics, 642, doi: [10.1051/0004-6361/202038130](https://doi.org/10.1051/0004-6361/202038130)

Oertel, M., Hempel, M., Klähn, T., & Typel, S. 2017, Rev. Mod. Phys., 89, 015007, doi: [10.1103/RevModPhys.89.015007](https://doi.org/10.1103/RevModPhys.89.015007)

Qin, P., Wang, S., Tong, H., et al. 2024, Phys. Rev. C, 109, 064603, doi: [10.1103/PhysRevC.109.064603](https://doi.org/10.1103/PhysRevC.109.064603)

Qu, X., Wang, S., & Tong, H. 2025, The Astrophysical Journal, 980, 3, doi: [10.3847/1538-4357/ada76b](https://doi.org/10.3847/1538-4357/ada76b)

Ramachandran, P., Zoph, B., & Le, Q. V. 2018, ArXiv, abs/1710.05941, <https://api.semanticscholar.org/CorpusID:10919244>

Russotto, P., Gannon, S., Kupny, S., et al. 2016, Phys. Rev. C, 94, 034608, doi: [10.1103/PhysRevC.94.034608](https://doi.org/10.1103/PhysRevC.94.034608)

Rutherford, N., Mendes, M., Svensson, I., et al. 2024, The Astrophysical Journal Letters, 971, L19, doi: [10.3847/2041-8213/ad5f02](https://doi.org/10.3847/2041-8213/ad5f02)

Salmi, T., Choudhury, D., Kini, Y., et al. 2024, The Astrophysical Journal, 974, 294, doi: [10.3847/1538-4357/ad5f1f](https://doi.org/10.3847/1538-4357/ad5f1f)

Sedrakian, A., Li, J. J., & Weber, F. 2023, Progress in Particle and Nuclear Physics, 131, 104041, doi: <https://doi.org/10.1016/j.ppnp.2023.104041>

Shen, S., Liang, H., Long, W. H., Meng, J., & Ring, P. 2019, Progress in Particle and Nuclear Physics, 109, 103713, doi: <https://doi.org/10.1016/j.ppnp.2019.103713>

Shen, S., Liang, H., Meng, J., Ring, P., & Zhang, S. 2017, Phys. Rev. C, 96, 014316, doi: [10.1103/PhysRevC.96.014316](https://doi.org/10.1103/PhysRevC.96.014316)

Sorensen, A., Agarwal, K., Brown, K. W., et al. 2024, Progress in Particle and Nuclear Physics, 134, 104080, doi: <https://doi.org/10.1016/j.ppnp.2023.104080>

Tong, H., Elhatisari, S., Meißner, U.-G., & Ren, Z. 2025a, Multi-strangeness matter from ab initio calculations. <https://arxiv.org/abs/2509.26148>

Tong, H., Elhatisari, S., & Meißner, U.-G. 2025b, Astrophys. J., 982, 164, doi: [10.3847/1538-4357/adba47](https://doi.org/10.3847/1538-4357/adba47)

Tong, H., Elhatisari, S., & Meißner, U.-G. 2025c, Science Bulletin, 70, 825, doi: <https://doi.org/10.1016/j.scib.2025.01.008>

Tong, H., Ren, X.-L., Ring, P., et al. 2018, Phys. Rev. C, 98, 054302, doi: [10.1103/PhysRevC.98.054302](https://doi.org/10.1103/PhysRevC.98.054302)

Tong, H., Wang, C., & Wang, S. 2022, The Astrophysical Journal, 930, 137, doi: [10.3847/1538-4357/ac65fc](https://doi.org/10.3847/1538-4357/ac65fc)

Tong, H., Wang, S., & Meng, J. 2025d, Frontiers in Astronomy and Space Sciences, Volume 12 - 2025, doi: [10.3389/fspas.2025.1666331](https://doi.org/10.3389/fspas.2025.1666331)

Tong, H., Zhao, P., & Meng, J. 2020, Physical Review C, 101, 035802, doi: [10.1103/PhysRevC.101.035802](https://doi.org/10.1103/PhysRevC.101.035802)

Traversi, S., & Char, P. 2020, The Astrophysical Journal, 905, 9, doi: [10.3847/1538-4357/abbfb4](https://doi.org/10.3847/1538-4357/abbfb4)

Tsang, C. Y., Tsang, M. B., Lynch, W. G., Kumar, R., & Horowitz, C. J. 2024, Nature Astronomy, 8, 328, doi: [10.1038/s41550-023-02161-z](https://doi.org/10.1038/s41550-023-02161-z)

van Dalen, E. N. E., Fuchs, C., & Faessler, A. 2005, Physical Review Letters, 95, 022302, doi: [10.1103/PhysRevLett.95.022302](https://doi.org/10.1103/PhysRevLett.95.022302)

Vinciguerra, S., Salmi, T., Watts, A. L., et al. 2024, The Astrophysical Journal, 961, 62, doi: [10.3847/1538-4357/acfb83](https://doi.org/10.3847/1538-4357/acfb83)

Wang, C., Hu, J., Zhang, Y., & Shen, H. 2020, The Astrophysical Journal, 897, 96, doi: [10.3847/1538-4357/ab994b](https://doi.org/10.3847/1538-4357/ab994b)

Wang, S., Tong, H., Wang, C., et al. 2024, Science Bulletin, 69, 2166, doi: <https://doi.org/10.1016/j.scib.2024.05.013>

Wang, S., Tong, H., Zhao, Q., et al. 2022a, Phys. Rev. C, 106, L021305, doi: [10.1103/PhysRevC.106.L021305](https://doi.org/10.1103/PhysRevC.106.L021305)

—. 2023, Phys. Rev. C, 108, L031303, doi: [10.1103/PhysRevC.108.L031303](https://doi.org/10.1103/PhysRevC.108.L031303)

Wang, S., Wang, C., & Tong, H. 2022b, Phys. Rev. C, 106, 045804, doi: [10.1103/PhysRevC.106.045804](https://doi.org/10.1103/PhysRevC.106.045804)

Wang, S., Zhao, Q., Ring, P., & Meng, J. 2021, Phys. Rev. C, 103, 054319, doi: [10.1103/PhysRevC.103.054319](https://doi.org/10.1103/PhysRevC.103.054319)

Wang, T., Tong, H., Wang, C., Qu, X., & Wang, S. 2025, Phys. Rev. C, 112, 054322, doi: [10.1103/2cn8-s9ss](https://doi.org/10.1103/2cn8-s9ss)

Weber, F., Negreiros, R., Rosenfield, P., & Stejner, M. 2007, Progress in Particle and Nuclear Physics, 59, 94, doi: <https://doi.org/10.1016/j.ppnp.2006.12.008>

Yang, J., & Piekarewicz, J. 2020, Annual Review of Nuclear and Particle Science, 70, 21, doi: <https://doi.org/10.1146/annurev-nucl-101918-023608>

Zhou, K., Wang, L., Pang, L.-G., & Shi, S. 2024, *Progress in Particle and Nuclear Physics*, 135, 104084,
doi: <https://doi.org/10.1016/j.ppnp.2023.104084>

Zhou, W., Hu, J., Zhang, Y., & Shen, H. 2023, *The Astrophysical Journal*, 950, 186,
doi: [10.3847/1538-4357/acd335](https://doi.org/10.3847/1538-4357/acd335)